ISSN 1023-1935, Russian Journal of Electrochemistry, 2013, Vol. 49, No. 12, pp. 1171–1180. © Pleiades Publishing, Ltd., 2013.
Original Russian Text © D.V. Korona, I.M. Kutikov, A.Ya. Neiman, 2013, published in Rusian in Elektrokhimiya, 2013, Vol. 49, No. 12, pp. 1305–1315.

Effect of Hydration on Conductivity of $Ba_4La_xCa_{2-x}Nb_2O_{11+0.5x}$ ($x = 0.5, 1, 1.5, 2$) Phases

D. V. Korona[z], I. M. Kutikov, and A. Ya. Neiman

Ural Federal University Named after the First President of Russia B.N. Eltsin, Lenina pr. 51, Ekaterinburg, 620083 Russia

Received July 18, 2011

Abstract—Substitution of Ca by La in initial cubic double perovskite $Ba_4(Ca_2Nb_2)O_{11}[V_O]_1$ allowed obtaining phases with a similar structure with a lower content of structural oxygen vacancies, $Ba_4(La_xCa_{2-x}Nb_2)O_{11+0.5x}[V_O]_{1-0.5x}$ ($x = 0.5, 1, 1.5, 2$). The impedance technique was used to measure the temperature dependences of conductivity in the atmosphere of dry and humid air. Transport numbers determined using the EMF method in an oxygen–air and water steam concentration cells point to the predominantly hole nature of conductivity in the high-temperature region ($T > 600$°C) and to predominance of proton conductivity in the low-temperature region. Activation energies of hole and proton conductivity were calculated. Thermogravimetric measurements were carried out under heating from 25 to 1000°C with simultaneous mass–spectrometric determination of evolved H_2O and CO_2. The properties of the studied $Ba_4(La_xCa_{2-x}Nb_2)O_{11+0.5x}$ ($x = 0.5, 1, 1.5, 2$) phases were compared with the earlier studied $Ba_{4-x}La_x(Ca_2Nb_2)O_{11+0.5x}$ phases with similar lanthanum content.

Keywords: double perovskite, oxygen vacancies, proton conductivity, impedance, transport numbers, thermogravimetry

DOI: 10.1134/S1023193512110079

INTRODUCTION

Transport properties and hydration of $Ba_{4-x}Ca_{2+x}Nb_2O_{11+0.5x}$ ($-0.62 \le x \le 0.82$) phases with the cubic double perovskite structure were studied as related to their possible application as proton conductors [1–5]. Also, $Ba_{4-x}La_xCa_2Nb_2O_{11+0.5x}$ ($0 \le x \le 1.5$) phases were studied in terms of proton conductivity. These are solid solutions obtained by substitution of barium by lanthanum in the $Ba_4Ca_2Nb_2O_{11}$ phase [6].

Owing to high tolerance of the double perovskite crystal lattice and presence of a considerable amount of structural oxygen vacancies (1/12 sites) in $Ba_4Ca_2Nb_2O_{11}$, there is a possibility of Ca substitution by La with preservation of the initial structure. This allows studying the effect of lanthanum content and structural oxygen vacancies on conductivity and the relevant properties of compounds with the composition of $Ba_4La_xCa_{2-x}Nb_2O_{11+0.5x}$.

In this connection, the aim of this work was to study conductivity of the $Ba_4La_xCa_{2-x}Nb_2O_{11+0.5x}$ ($x = 0.5, 1, 1.5, 2$) phase in the atmosphere of dry and humid air and measure the transport number using the EMF technique. The activation energy of hole conductivity and also that of proton conductivity predominant at low temperature and high humidity was calculated. The method of thermogravimetry was used to study water intercalation with the filling of oxygen vacancies and determine the hydration degree.

EXPERIMENTAL

The studied $Ba_4(La_xCa_{2-x}Nb_2)O_{11+0.5x}[V_O]_{1-0.5x}$ ($x = 0.5, 1, 1.5, 2$) compositions were obtained on the basis of the corresponding oxides and carbonates (ultra high purity grade) by means of solid–phase synthesis according to a ceramic technology with 4 stages and stepwise temperature increase from 800 to 1300°C. Presence of a single phase in the obtained ceramic was established using the XRD technique (Bruker D8 ADVANCE diffractometer, Cu$K\alpha$ radiation, angle range of $2\theta = 10°–80°$).

Impedance measurements were carried out using the double-contact technique in the frequency range of 100 Hz–1 MHz with the help of a Z-1000P impedance meter (Ellins).

Samples for measurement of conductivity were disks of 10 × 2 mm obtained by uniaxial compaction and the sintering at 1500°C for 12 h. A platinum powder suspension in an alcohol solution of colophony was used for application of Pt electrodes on ground sample end surfaces. The electrode sintering was carried out for 3 h at 1100°C.

The atmosphere with a given humidity was provide by air circulation (P_{O_2} = 21 kPa) through zeolites

[z] Corresponding author: Danil.Korona@usu.ru (D.V. Korona).

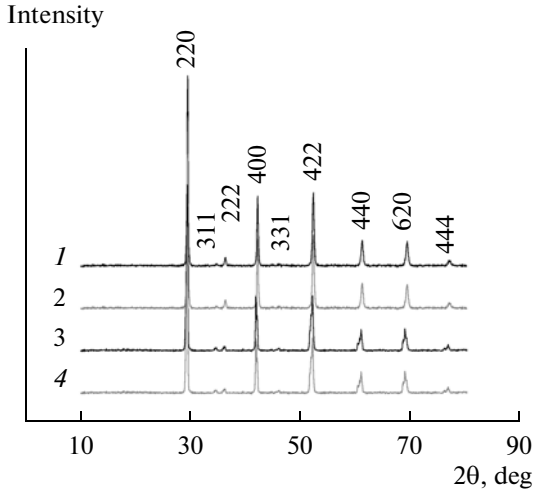

Fig. 1. X-ray patterns of $Ba_4La_xCa_{2-x}Nb_2O_{11+0.5x}$: (*1*) $Ba_4La_{0.5}Ca_{1.5}Nb_2O_{11.25}$ ($x = 0.5$), (*2*) $Ba_4LaCaNb_2O_{11.5}$ ($x = 1$), (*3*) $Ba_4La_{1.5}Ca_{0.5}Nb_2O_{11.75}$ ($x = 1.5$), (*4*) $Ba_4La_2Nb_2O_{12}$ ($x = 2$).

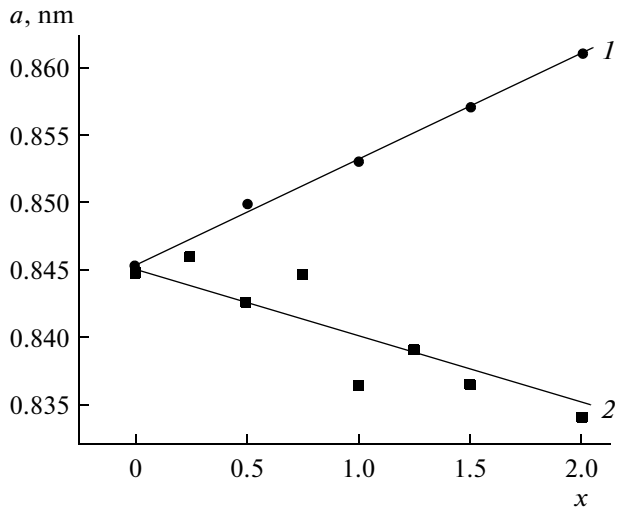

Fig. 2. Dependence of cubic lattice parameter a on lanthanum content x for the following phases: (*1*) $Ba_4La_xCa_{2-x}Nb_2O_{11+0.5x}$; (*2*) $Ba_{4-x}La_xCa_2Nb_2O_{11+0.5x}$.

NaAX ($\log P_{H_2O} = -6.5$, a dry atmosphere) and saturated KBr solution ($\log P_{H_2O} = -1.9$, a humid atmosphere). Humidity was controlled using an IVG-1 MK-S meter of gas humidity (Exis).

Thermogravimetric studies were carried out in the course of heating at the rate of 10°/min in the temperature range of 30–1000°C in a atmosphere of dry Ar on a STA 409 PC Luxx thermal analyzer (Netzsch). Analysis of evolved gases was performed using a QMS 403C Aëlos quadrupole mass spectrometer (Netzsch) connected serially to the thermal analyzer.

Ground powders of compounds were conditioned for 24 h at the temperature of 200°C in a humid atmosphere (relative humidity of 80%) to achieve the maximum hydration degree. Then the samples were subjected to dehydration under heating at the rate of 10°/min in a dry argon atmosphere. Thermogravimetry was used to determine the hydration degree (amount of mols of water per 1 mol of the substance) of $Ba_4La_xCa_{2-x}Nb_2O_{11+0.5x}$ ($x = 0.5$, 1, 1.5, 2).

Transport numbers were determined using the EMF technique. The method was based on measurement of electromotive force of the concentration cell where the studied substance sample was used as electrolyte. If a gradient of partial oxygen pressure is applied on electrolyte, then EMF of the concentration cell is:

$$E_{meas} - E_0 = \frac{RT}{4F}\bar{t}_{ion}\ln\frac{P(O_2)''}{P(O_2)'}, \quad (1)$$

where E_{meas} is the measured EMF value under the $P(O_2)$ gradient, E_0 is the difference in the cell potentials in the absence of the gradient, at $P(O_2)' = P(O_2)''$, $\bar{t}_{ion}$ is the overall transport number of all ions.

If a gradient of partial pressure of water vapor (at $P(O_2)' = P(O_2)''$) is applied on electrolyte, then EMF of the concentration cell is [7]:

$$E_{meas} - E_0 = \frac{RT}{2F}\bar{t}_H\ln\frac{P(H_2O)''}{P(H_2O)'}, \quad (2)$$

where E_{meas} is the measured EMF value under the $P(H_2O)$ gradient, E_0 is the difference in the cell potentials at $P(H_2O)' = P(H_2O)''$, $\bar{t}_H$ is the transport number of protons. Thus, the EMF method was used to determine the average transport numbers of the carriers in the range of $P(O_2) = 100...21$ kPa or $P(H_2O) = 100...300$ Pa.

RESULTS AND DISCUSSION

XRD and Ceramic Morphology

X-ray patterns (Fig. 1) obtained for dehydrated samples showed that the studied compositions contain a single phase with impurity content below 3%. All obtained phases have a cubic double perovskite structure. The lattice parameters are given in Fig. 2. An increase in La content results in a monotonous increase in the crystal lattice parameter, which cannot be explained only by the difference in the radii of Ca and La atoms (they are very close, see Table 1). An increase in x in $Ba_4(La_xCa_{2-x}Nb_2)O_{11+0.5x}[V_O]_{1-0.5x}$ leads to the filling of structural oxygen vacancies. Herewith, the oxygen ion filling the vacancy "expands" the neighboring oxygen ions, which results in an increase in the lattice cell parameter.

For comparison, Fig. 2 (curve *2*) also presents the dependence of the lattice parameter for $Ba_{4-x}La_xCa_2Nb_2O_{11+0.5x}$. The lattice parameter

decreases under increasing barium substitution by lanthanum, as the radius of La^{3+} is much lower than the radius of Ba^{2+}.

The color of ceramic caked samples with the composition of $Ba_4La_xCa_{2-x}Nb_2O_{11+0.5x}$ changed at an increase in lanthanum content from light gray (x = 0.5) to dark gray (x = 1.5), except for the sample with x = 2, also with a light gray color. Relative density of the ceramic decreases at an increase in x and is minimal for the sample with x = 2.

Measurement of Sample Resistance: Estimation of Establishment of Equilibrium and Impedance Spectra

Figure 3 shows the data characterizing the time in which the equilibrium resistance value is reached at stepwise temperature variation; one can see that the dependences are different in a dry and humid atmosphere.

The time in which the equilibrium resistance value is reached in a dry atmosphere is 10 h at the temperature of 390°C and 50 h at the temperature of 370°C. Therefore, resistance measurements are problematic at low temperatures due to very slow establishment of equilibrium.

No equilibrium is reached in a humid atmosphere at the temperature below 390°C, as linear increase in the grain boundary resistance is observed (as follows from the impedance data) as a result of surface sample hydrolysis.

Resistance measurement using the impedance technique allowed determining the contribution of the grain bulk and boundaries into the overall sample resistance. Figure 4 shows examples of the impedance complex plane plots, where three semicircles can be distinguished corresponding to the bulk, grain boundary, and electrode resistance. The high-frequency section of the obtained impedance spectra allows calculating the bulk resistance.

Table 1. Radii of cations for coordination numbers 6 and 12 [8, 9]

Coordination number	Ba^{2+}, nm	La^{3+}, nm	Ca^{2+}, nm	Nb^{5+}, nm
12	0.161	0.136	0.134	
6		0.103	0.10	0.064

Temperature Dependences of Bulk Conductivity

Figure 5 shows temperature dependences of bulk conductivity for $Ba_4La_xCa_{2-x}Nb_2O_{11+0.5x}$ (x = 0.5, 1, 1.5, 2) phases in a dry and humid atmosphere as compared to $Ba_4Ca_2Nb_2O_{11}$ (x = 0). High-temperature and low–temperature sections can be found in the presented dependences. The high-temperature linear section (approximately 900–600°C) is better pronounced in a dry atmosphere. The low-temperature section is nonlinear due to an increase in the concentration of protons owing to hydration. For phases with x = 0, 0.5, 1, 1.5, close conductivity values are observed in the high-temperature linear region at a high temperature. The phase with x = 2, in which structural oxygen vacancies are absent, is characterized by bulk conductivity lower by 2 orders of magnitude as compared to other phases.

In a humid atmosphere, overall conductivity is higher due to appearance of the proton conductivity contribution. The highest difference between conductivity in a dry and humid atmosphere corresponds to the $Ba_4La_{0.5}Ca_{1.5}Nb_2O_{11.25}$ phase. The lowest effect is produced by humidity on conductivity of the $Ba_4La_2Nb_2O_{12}$ phase.

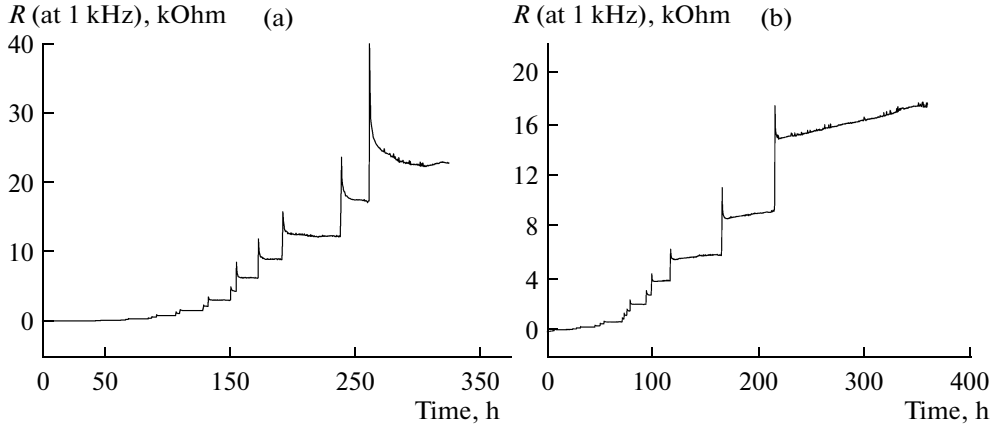

Fig. 3. Dependences of variation of resistance on time at a stepwise temperature decrease for $Ba_4La_{0.5}Ca_{1.5}Nb_2O_{11.25}$: (a) in a dry atmosphere, $\log P_{H_2O} = -6.5$; (b) in a humid atmosphere, $\log P_{H_2O} = -1.9$.

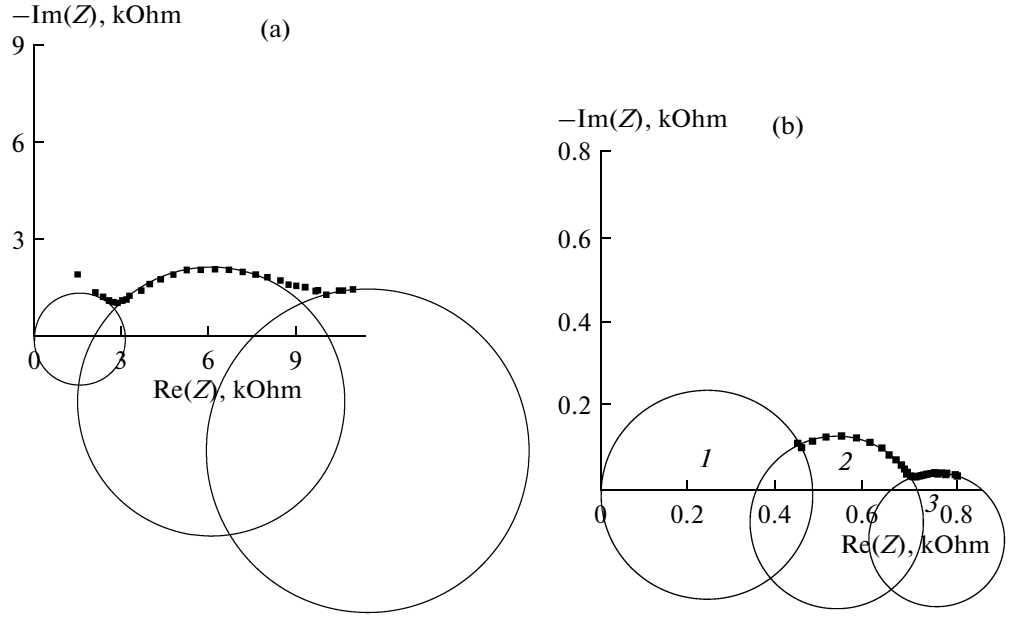

Fig. 4. Impedance complex plane plots for $Ba_4La_{1.5}Ca_{0.5}Nb_2O_{11.75}$: (a) in a dry atmosphere at $T = 416°C$; (b) in a humid atmosphere at $T = 685°C$.

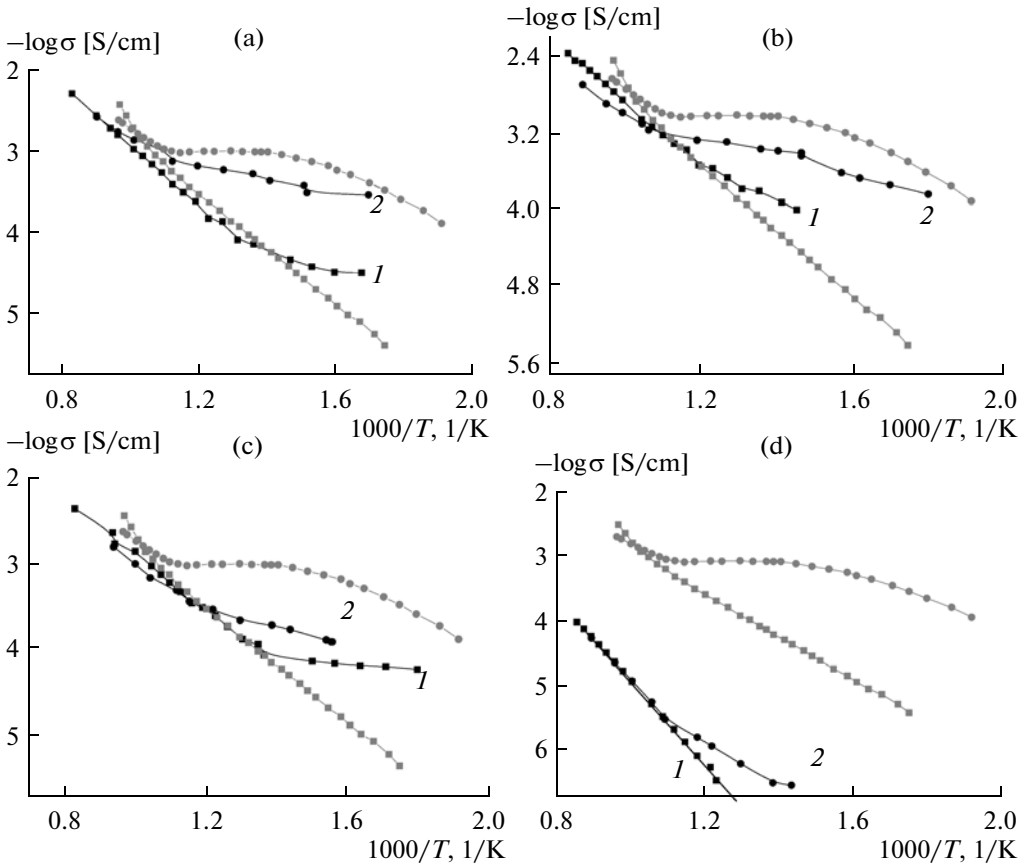

Fig. 5. Temperature dependences of conductivity in (*1*) a dry and (*2*) humid atmosphere for: $Ba_4La_{0.5}Ca_{1.5}Nb_2O_{11.25}$ (a); $Ba_4La_1Ca_1Nb_2O_{11.5}$ (b); $Ba_4La_{1.5}Ca_{0.5}Nb_2O_{11.75}$ (c); $Ba_4La_2Nb_2O_{12}$ (d) as compared to $Ba_4Ca_2Nb_2O_{11}$. The data for $Ba_4Ca_2Nb_2O_{11}$ are shown in gray.

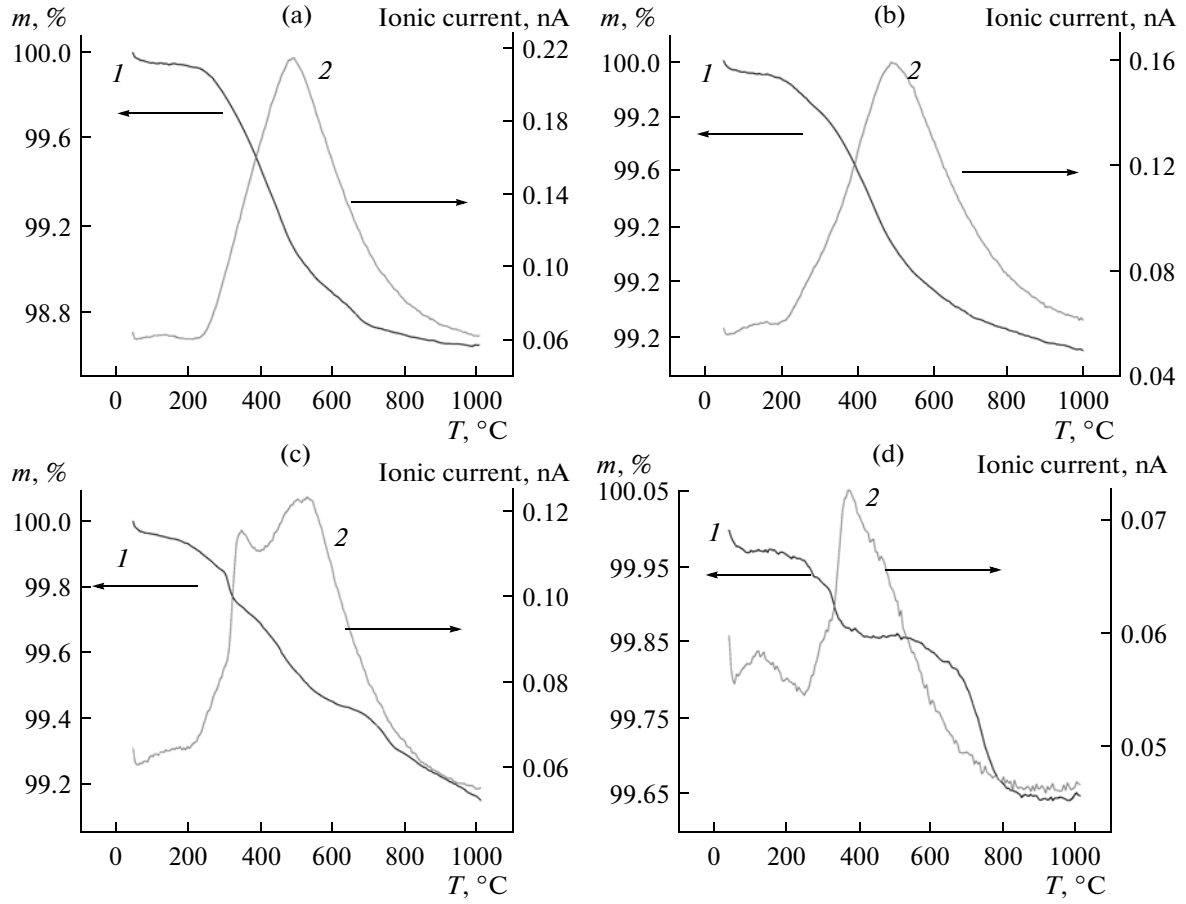

Fig. 6. (*1*) Results of thermogravimetry; (*2*) data of mass spectrometry for water: (a) $Ba_4La_{0.5}Ca_{1.5}Nb_2O_{11.25}$; (b) $Ba_4La_1Ca_1Nb_2O_{11.5}$; (c) $Ba_4La_{1.5}Ca_{0.5}Nb_2O_{11.75}$; (d) $Ba_4La_2Nb_2O_{12}$.

Thermogravimetry of $Ba_4La_xCa_{2-x}Nb_2O_{11+0.5x}$ ($x = 0.5, 1, 1.5, 2$)

Under heating, a significant mass loss by all samples was observed (Fig. 6). According to the mass spectrometry data, one can see two peaks of water elimination: at 360°C (water chemosorbed on the grain surface is eliminated) and 490°C (water from structural oxygen vacancies V_O^X is eliminated). For samples with $x = 0.5$ and $x = 1$, mass loss is mainly determined by water elimination from structural vacancies, the peak of H_2O elimination is at 490°C. The two peaks of H_2O elimination are approximately similar for the sample with $x = 1.5$, while for $x = 2$, the peak of H_2O at 360°C is present, but the peak at 490°C is absent due to the absence of structural oxygen vacancies. It should be noted that peaks of CO_2 evolution at 700°C are observed for samples with $x = 1.5$ and $x = 2$ due to penetration of carbon dioxide admixtures from the atmosphere into the samples.

As seen in Fig. 7, the maximum hydration degree for $Ba_4La_xCa_{2-x}Nb_2O_{11+0.5x}$ compounds with $x = 0.5$ corresponds to the complete filling of structural oxygen vacancies by water molecules.

For compounds with a lower content of oxygen vacancies ($x = 1$, 1.5, and 2) V_O^X, the maximum hydration degree exceeds the V_O^X content by approximately 0.1 mol/mol. This means that water chemosorption on the sample grain surface (grain diameter of 1–10 μm) is observed after the filling of structural vacancies. This excess of sorbed water is removed at 360°C.

Results of Measurement of Transport Numbers Using EMF Method for $Ba_{4-x}La_xCa_2Nb_2O_{11+0.5x}$

Measurements of the overall ionic ($t_{ion} \approx t_O + t_H$) and protonic ($t_H$) transport numbers were carried out using the EMF method for barium–calcium niobates with partial substitution of barium by lanthanum $Ba_{3.5}La_{0.5}Ca_2Nb_2O_{11.25}$, $Ba_3LaCa_2Nb_2O_{11.5}$, and $Ba_{2.5}La_{1.5}Ca_2Nb_2O_{11.75}$ (Fig. 8).

For two compounds ($Ba_{3.5}La_{0.5}Ca_2Nb_2O_{11.25}$ and $Ba_{2.5}La_{1.5}Ca_2Nb_2O_{11.75}$), overall ionic ($t_{ion} \approx t_O + t_H$) and protonic transport numbers (t_H) measured using the EMF method in oxygen–air and water–steam cells, accordingly, are shown in the figure as compared to ionic transport numbers calculated on the basis of

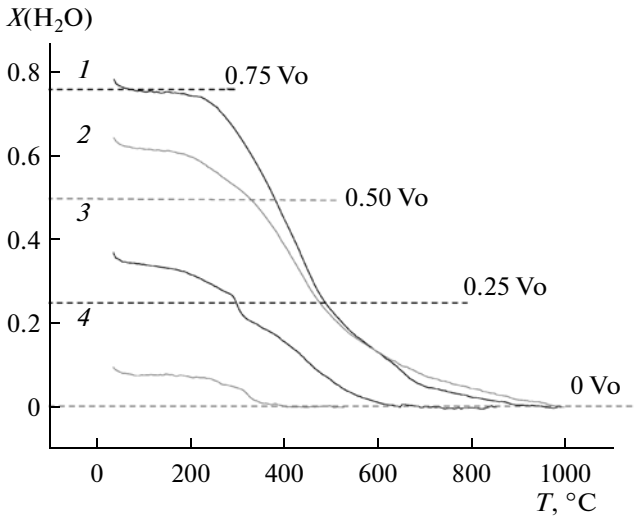

Fig. 7. Temperature dependences of hydration degree of $Ba_4La_xCa_{2-x}Nb_2O_{11+0.5x}[V_O^X]_{1-0.5x}$ ($x = 0.5, 1, 1.5, 2$) samples with a different content of oxygen vacancies: (*1*) $Ba_4La_{0.5}Ca_{1.5}Nb_2O_{11.25}[V_O^X]_{0.75}$ ($x = 0.5$); (*2*) $Ba_4La_1Ca_1Nb_2O_{11.5}[V_O^X]_{0.5}$ ($x = 1$); (*3*) $Ba_4La_{1.5}Ca_{0.5}Nb_2O_{11.75}[V_O^X]_{0.25}$ ($x = 1.5$), (*4*) $Ba_4La_2Nb_2O_{12}[V_O^X]_0$ ($x = 2$).

dependences of conductivity on $P(O_2)$. The method of calculating ionic transport numbers and experimental data are described in [6]. The calculated transport numbers of ions correspond to a dry atmosphere with $\log P(H_2O) = -4$. The overall transport number of ions was measured using the EMF method in a humid atmosphere with $\log P(H_2O) = -2.5$. As seen in Figs. 8a, 8b, the measured and calculated transport numbers agree satisfactorily. As in the case of the $Ba_{3.5}La_{0.5}Ca_2Nb_2O_{11.25}$ sample (Fig. 8a) with a low lanthanum content and accordingly high content of vacancies, different methods yield an approximately similar result regarding transport numbers at a high temperature. At a decrease in the temperature, the data fall apart, as ionic transport numbers are higher in a humid atmosphere. For the $Ba_{2.5}La_{1.5}Ca_2Nb_2O_{11.75}$ sample (Fig. 8c) (with a high lanthanum content and accordingly low content of vacancies), the measured and calculated ionic transport numbers in a dry and humid atmosphere approximately coincide. The overall ionic and protonic transport numbers grow negligibly at a decrease in the temperature due to intercalation of a small amount of water.

It should also be noted that the overall ionic transport numbers grow faster than protonic transport numbers at a decrease in the temperature. Herewith, below 600°C, the Σt_{ion} values exceed unity, which points to absence of equilibrium by oxygen on electrodes due to their low reversibility.

Comparison of Measured and Calculated Transport Numbers of $Ba_4La_xCa_{2-x}Nb_2O_{11+0.5x}$ ($x = 0.5, 1, 1.5$)

Overall ionic and protonic transport numbers were measured using the EMF method (Fig. 9) for barium–calcium niobates with partial barium substitution by lanthanum $Ba_4La_{0.5}Ca_{1.5}Nb_2O_{11.25}$ ($x = 0.5$), $Ba_4LaCaNb_2O_{11.5}$ ($x = 1$), and $Ba_4La_{1.5}Ca_{0.5}Nb_2O_{11.75}$ ($x = 1.5$). For the $Ba_4La_2Nb_2O_{12}$ ($x = 2$) phase, measurements are problematic due to its low conductivity.

Protonic transport numbers measured using the EMF method can be complemented by calculated data, as follows from the dependence of overall conductivity ($\sigma_{overall} = \sigma_H + \sigma_h + \sigma_O$) on the temperature. In the high-temperature range ($\sigma_{overall} \approx \sigma_h + \sigma_O$), the dependences of $\log\sigma_{overall} = f(1/T)$ are linear. A decrease in the temperature results in deviation of the dependence from linearity due to appearance of protonic conductivity σ_H. In the calculation, the linear high-temperature section of the dependence of $\log\sigma_{overall} = f(1/T)$ (corresponding to $\sigma_h + \sigma_O$) was extrapolated to low temperatures. Then protonic conductivity $\sigma_H = \sigma_{overall} - (\sigma_h + \sigma_O)$ and transport numbers $t_H = \sigma_H/\sigma_{overall}$ were calculated.

As seen in the dependences presented in Fig. 9, calculation on the basis of the conductivity data yields understated values of protonic transport numbers at a high temperature. On the other hand, the EMF method understates at low temperatures the values of protonic transport numbers and overstates ionic transport numbers. Thus, the two methods complement each other: the EMF method yields more exact values of transport numbers at high temperatures (above 600°C) and the calculation allows obtaining more exact data below 600°C.

All the studied compounds in air atmosphere are predominantly hole conductors ($t_h = 0.7–0.9$) at the high temperature, ≥700°C, and become mainly protonic conductors ($t_H = 0.7–0.9$) at the temperature of ≤400°C. For all compounds, the overall ionic ($t_O + t_H$) and protonic transport numbers t_H grow at a decrease in the temperature.

Dependence of Transport Numbers on Lanthanum Content (Content of Oxygen Vacancies)

As follows from the data in Fig. 10, the overall ionic transport numbers $t_{(O+H)}$ decrease (hole conductivity increases) and protonic transport numbers t_H grow for all compounds at a decrease in lanthanum content x (increase in vacancy content).

Thus, an increase in the vacancy content results in an increase in the level of protonic and hole conductivity. At an increase in the content of structural oxygen vacancies, equilibrium in quasichemical reactions

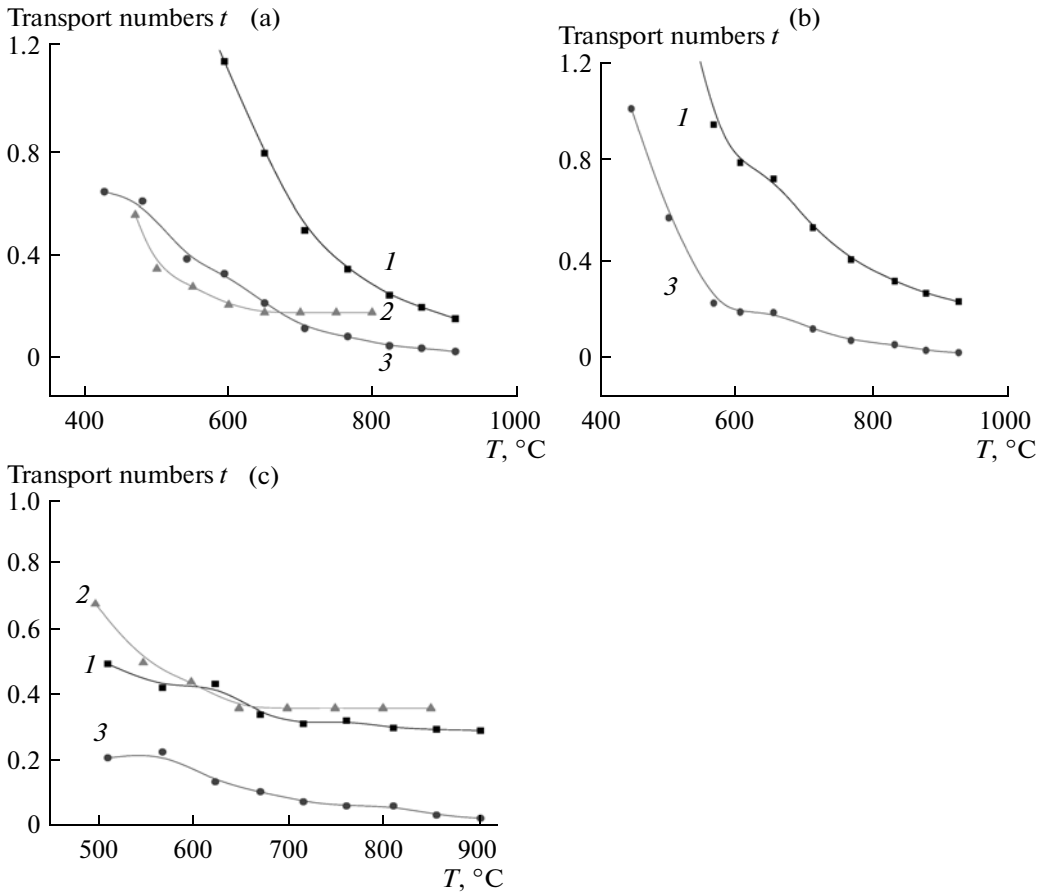

Fig. 8. Dependences on the temperature of transport numbers for $Ba_{4-x}La_xCa_2Nb_2O_{11+0.5x}$: (a) $x = 0.5$; (b) $x = 1$; (c) $x = 1.5$; at different humidity values: (*1*) overall ionic ones at $\log(pH_2O) = -2.5$; (*2*) calculated overall ionic $\overline{T}_{ion}$ at $\log(pH_2O) = -4$; (*3*) protonic t_H at $\log(pH_2O) = -2.5$.

of mobile defect formation (4)–(6) shifts to the right, towards formation of protons and holes.

$$V_O^X + O_O^X \leftrightarrow V_O^{\bullet\bullet} + O_V'', \quad (4)$$

$$1/2O_2 + V_O^{\bullet\bullet} + O_V'' \leftrightarrow O_O^X + 2h^{\bullet} + O_V'', \quad (5)$$

$$H_2O + V_O^{\bullet\bullet} + O_V'' + O_O^X \leftrightarrow O_V'' + 2(OH)_O^{\bullet}. \quad (6)$$

Dependences of Hole–Oxygen Conductivity and Activation Energy of Lanthanum Content

From the high-temperature linear section of the temperature dependences of conductivity in a dry atmosphere (Fig. 5) re-constructed in the $\log(\sigma T)$, $1/T$ coordinates, activation energies E_a of hole–oxygen conductivity are calculated.

As seen in Fig. 11, one can see that the obtained dependences are different for the studied $Ba_4La_xCa_{2-x}Nb_2O_{11+0.5x}$ (x = 0.5, 1, 1.5, 2) phases and the earlier studied $Ba_{4-x}La_xCa_2Nb_2O_{11+0.5x}$ (x = 0.5, 1, 1.5) phases [6]. For phases with Ca substitution by La, the activation energy and conductivity change negligibly (except for the composition with full absence of vacancies) at an increase in lanthanum content up to the $Ba_4La_2Nb_2O_{12}$ (x = 2) phase, for which E_a grows stepwise. The conductivity level of $Ba_4La_2Nb_2O_{12}$ is approximately two orders of magnitude lower and the activation energy is approximately twice higher than in other phases from the $Ba_4La_xCa_{2-x}Nb_2O_{11+0.5x}$ range. This is due to the fact that formation of mobile charge carriers according to equations (4)–(6) becomes impossible due to the absence of V_O.

For phases with Ba substitution by La, the activation energy grows monotonously at an increase in x and conductivity decreases accordingly.

The dependences of properties on the composition in Fig. 11 cannot be explained only by a decrease in the content of structural vacancies at an increase in La content, which causes a decrease in conductivity and an increase in the activation energy (this factor affects similarly both families of solid solutions). To explain the obtained regularities, one should take into account such a factor as variation of the lattice parameter at an increase in x. As seen from comparison of the data in Fig. 11 and Fig. 2, the data in Fig. 11 can be explained

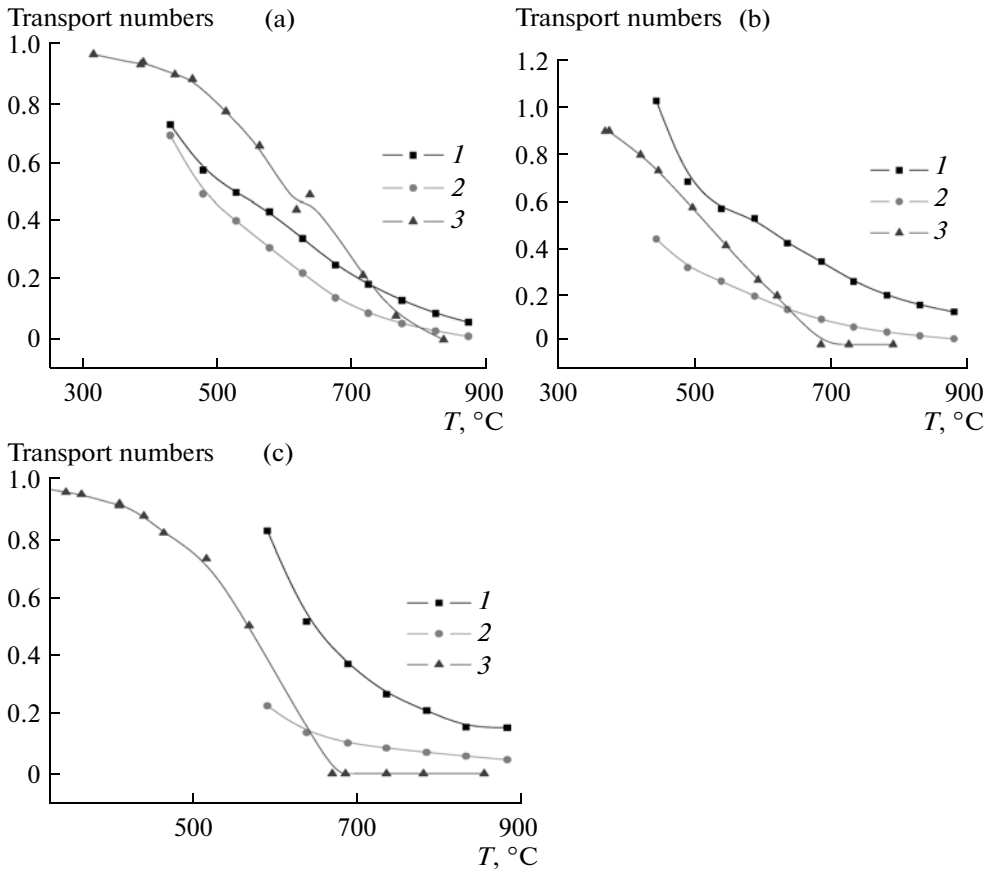

Fig. 9. Dependences on the temperature of transport numbers for $Ba_4La_xCa_{2-x}Nb_2O_{11+0.5x}$: (a) $x = 0.5$; (b) $x = 1$; (c) $x = 1.5$; at different humidity values: (*1*) overall ionic ones at $\log(pH_2O) = -2.5$; (*2*) protonic t_H at $\log(pH_2O) = -2.5$; (*3*) calculated protonic t_H at $\log(pH_2O) = -1.7$.

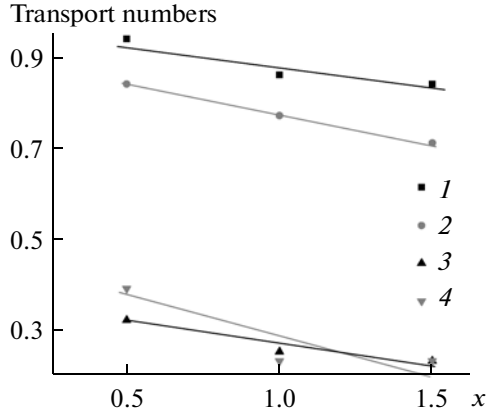

Fig. 10. Dependences of transport numbers on content of the La impurity: (*1*) the fraction of hole transport t_h in $Ba_{4-x}La_xCa_2Nb_2O_{11+0.5x}$ at 900°C; (*2*) t_h in $Ba_4La_xCa_{2-x}Nb_2O_{11+0.5x}$ at 900°C; (*3*) the fraction of protonic transport t_H in $Ba_{4-x}La_xCa_2Nb_2O_{11+0.5x}$ at 470°C; (*4*) t_H in $Ba_4La_xCa_{2-x}Nb_2O_{11+0.5x}$ at 470°C.

by superposition of the effect of structural vacancy content and lattice parameter variation.

Calculation of Activation Energy of Protonic Conductivity

The equation for ionic conductivity is known from the literature [10]:

$$\sigma_i = q_i c_i c(V_i) \nu_i^2 r_i \exp[-E_a/(kT)]/(kT), \qquad (7)$$

where ν is the frequency of hopping attempts, r is the average hopping length, q is the ion charge, N_A is the Avogadro constant, V is the volume, k is the Boltzmann constant, E_a is the conductivity activation energy, T is the absolute temperature, c_i is the concentration of the active form of the charge carrier component i, $c(V_i)$ is the concentration of sites available for charge carrier component i.

A specific feature of protonic conductivity consists in the fact that the concentration of protons depends on the temperature $c_H(T)$ and increases at a decrease in the temperature due to hydration. Therefore, the data of thermogravimetry ($c_H(T)$) and measurements of transport numbers ($t_H = \sigma_H/\sigma_{overall}$) should be used

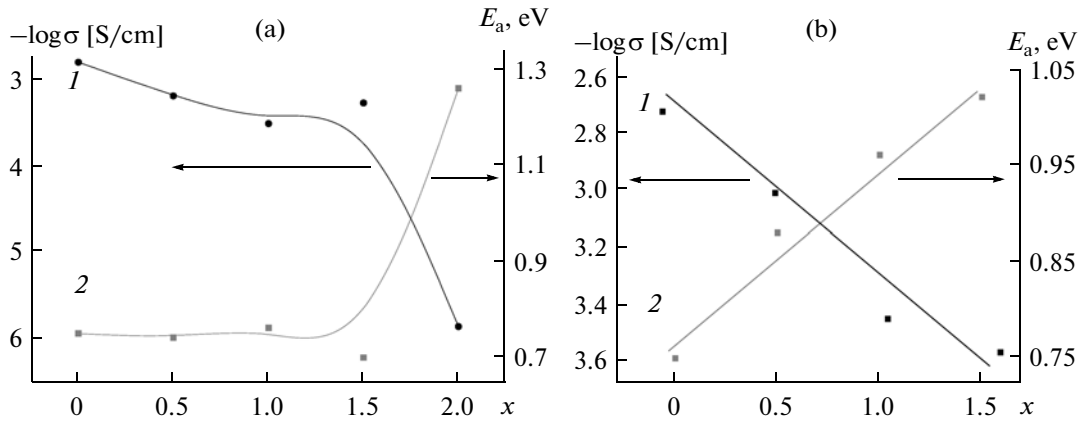

Fig. 11. Dependences of (*1*) conductivity and (*2*) activation energy on La content (x) for the following phases: (a) $Ba_4La_xCa_{2-x}Nb_2O_{11+0.5x}$; (b) $Ba_{4-x}La_xCa_2Nb_2O_{11+0.5x}$ at 700°C.

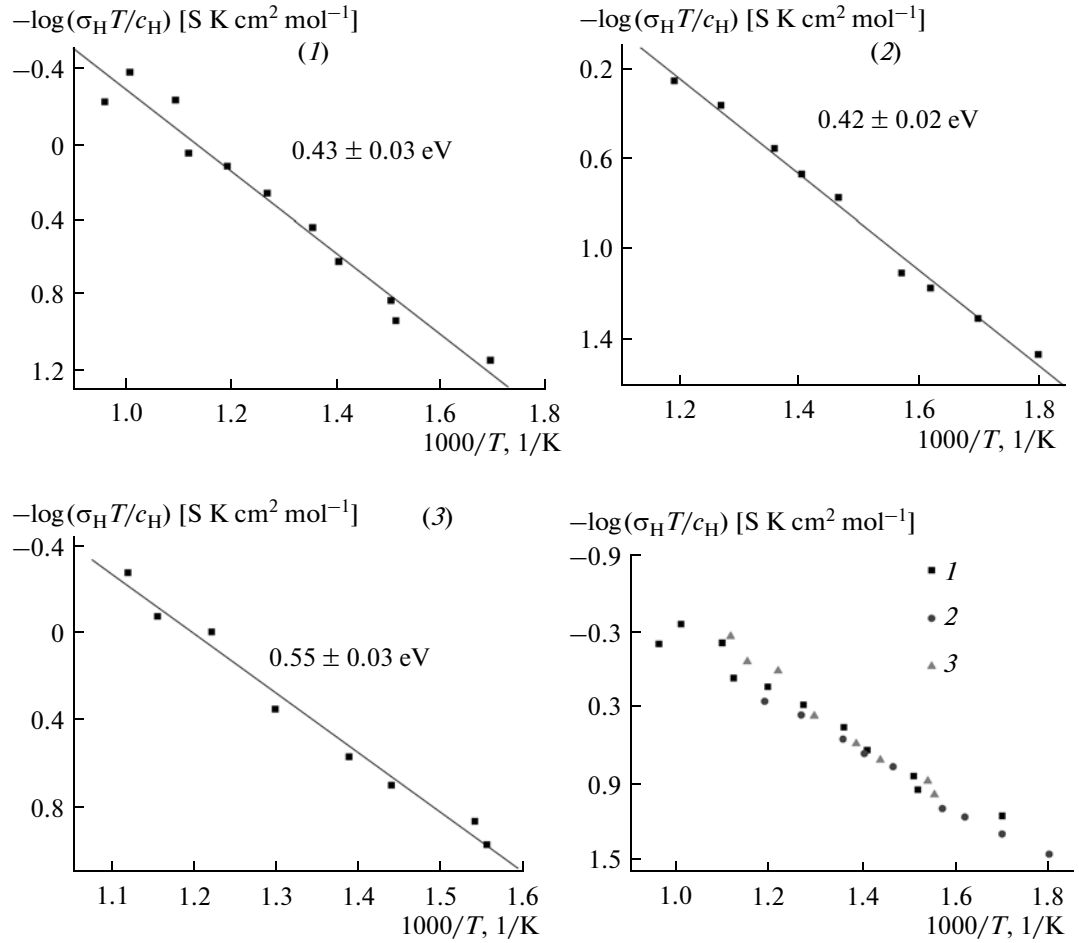

Fig. 12. Temperature dependences and activation energies of protonic conductivity: (*1*) $Ba_4La_{0.5}Ca_{1.5}Nb_2O_{11.25}$; (*2*) $Ba_4La_1Ca_1Nb_2O_{11.5}$; (*3*) $Ba_4La_{1.5}Ca_{0.5}Nb_2O_{11.75}$.

Table 2. Parameters of phase structures and density of ceramic samples

Sample composition	Molar mass, g/mol	Cubic lattice parameter, nm	Measured density, g/cm^3	X-ray density, g/cm^3	Relative sample density
$Ba_4La_{0.5}Ca_{1.5}Nb_2O_{11.25}$	1204.94	0.850 ± 0.004	5.488	6.252	0.877
$Ba_4La_1Ca_1Nb_2O_{11.5}$	1151.524	0.853 ± 0.004	5.213	6.062	0.859
$Ba_4La_{1.5}Ca_{0.5}Nb_2O_{11.75}$	1098.109	0.857 ± 0.004	4.823	5.873	0.821
$Ba_4La_2Nb_2O_{12}$	1044.693	0.861 ± 0.004	4.095	5.643	0.725

together for estimation of the activation energy of protonic conductivity. To eliminate the effect of the c_H dependence on the temperature, one should divide the corresponding $\sigma_H(T)$ values by $c_H(T)$ at each temperature and construct the $\log\left(T\frac{\sigma_H}{c_H}\right) = A - \frac{B}{T}$ straight line. As a result of protonic conductivity in $Ba_4La_xCa_{2-x}Nb_2O_{11+0.5x}$ ($x = 0.5$, 1, 1.5), activation energies of ≈0.42–0.55 eV were obtained (Fig. 12), which is close to the literature data for $Ba_4Ca_2Nb_2O_{11}$ (0.55 eV) and also to $Ba_3Ca_{1.18}Nb_{1.82}O_{8.73}$ (0.45 eV). As seen from the cumulative plot (curve *1*, *2*, *3* in Fig. 12), protonic mobilities (conductivities per proton concentration) are approximately similar for the three phases. Thus, mobility of protons in these phases is practically independent of the concentration of structural oxygen vacancies.

CONCLUSIONS

Substitution of La → Ca in the $Ba_4Ca_2Nb_2O_{11}$ phase yielded single–phase solid solutions with the overall formula of $Ba_4La_xCa_{2-x}Nb_2O_{11+0.5x}[V_O^X]_{1-0.5x}$ ($x = 0.5$, 1, 1.5, 2) with a double perovskite structure. The cubic lattice parameter for the studied $Ba_4La_xCa_{2-x}Nb_2O_{11+0.5x}[V_O^X]_{1-0.5x}$ grows at an increase in x and decrease in $[V_O^X]$, as opposed to the earlier studied $Ba_{4-x}La_xCa_2Nb_2O_{11+0.5x}[V_O^X]_{1-0.5x}$, for which the parameter diminishes at an increase in x.

High-temperature (predominantly, hole) conductivity of phases with substitution of Ca by La ($Ba_4La_xCa_{2-x}Nb_2O_{11+0.5x}$) is compared with similar phases with substitution of Ba by La ($Ba_{4-x}La_xCa_2Nb_2O_{11+0.5x}$). For the earlier studied $Ba_{4-x}La_xCa_2Nb_2O_{11+0.5x}[V_O^X]_{1-0.5x}$, conductivity diminishes monotonously at a decrease in $[V_O^X]$ content, as opposed to the studied $Ba_4La_xCa_{2-x}Nb_2O_{11+0.5x}[V_O^X]_{1-0.5x}$, for which conductivity remains practically unchanged at a decrease in $[V_O^X]$, except for $Ba_4La_2Nb_2O_{12}$. Thus, it should be pointed out that the hole–oxygen conductivity of these phases is considerably affected not only by content of structural oxygen vacancies, but also the value of the crystal lattice parameter.

For $Ba_4La_xCa_{2-x}Nb_2O_{11+0.5x}$ and $Ba_{4-x}La_xCa_2Nb_2O_{11+0.5x}$ ($x = 0.5$, 1, 1.5) phases, the overall ionic and protonic transport numbers were measured using the EMF method and the values were compared with the calculated ones. It is shown that for all $Ba_4La_xCa_{2-x}Nb_2O_{11+0.5x}[V_0]_{1-0.5x}$ ($x = 0.5$, 1, 1.5, 2) compositions, conductivity in a dry air atmosphere in the main section is hole conductivity. Overall conductivity grows in humid atmosphere due to appearance of protonic conductivity. One can point out the common regularity for the both solid solutions consisting in an increase in both hole and protonic conductivity at an increase in content of structural oxygen vacancies (at a decrease in La content).

ACKNOWLEDGMENTS

The work was supported by the Russian Foundation for Basic Research (projects no. 10-03-01149-a and 08-03-00144) and Ministry of Education and Science of the Russian Federation under the Federal Target Program "Scientific and Scientific–Pedagogical Resources of Innovative Russia in 2009–2013," and Federal Target Program "Development of Scientific Potential of the Higher School in 2009–2010."

REFERENCES

1. Animitsa, I., Neiman, A., Kochetova, N., Melekh, B., and Sharafutdinov, A., *Solid State Ionics*, 2003, vol. 162–163, p. 63.
2. Animitsa, I.E., Neiman, A.Ya., Kochetova, N.A., and Korona, D.V., *Russ. J. Electrochem.*, 2006, vol. 42, p. 311.
3. Animitsa, I., Denisova, T., Neiman, A., Nepryahin, A., Kochetova, N., Zhuravlev, N., and Colomban, Ph., *Solid State Ionics*, 2003, vol. 162–163, p. 73.
4. Colomban, Ph., Romain, F., Neiman, A., and Animitsa, I., *Solid State Ionics, 2*001, vol. 145, p. 339.
5. Korona, D.V., Neiman, A.Ya., Animitsa, I.E., and Sharafutdinov, A.R., *Russ. J. Electrochem.*, 2009, vol. 45, p. 586.
6. Korona, D.V. and Neiman, A.Ya., *Russ. J. Electrochem.*, 2011, vol. 47, p. 737.
7. Norby, T., *Solid State Ionics*, 1988, vol. 28–30, p. 1586.
8. Shannon, R.D., *Acta Crystallogr.*, 1976, vol. A32, p. 751.
9. Jia, Y.Q., *J. Solid State Chem.*, 1991, vol. 95, p. 184.
10. Chebotin, V.N. and Perfil'ev, M.V., *Elektrokhimiya tverdykh elektrolitov* (Electrochemistry of Solid Electrolytes), Moscow: Khimiya, 1978.